Solvatomorphs of $(Bu_4N)_2[\{Ag(N_2\text{-}py)\}_2Mo_8O_{26}]$: structure, colouration and phase transition

Pavel A. Abramov,*[a] Vladislav Yu. Komarov,[a] Denis A. Pischur,[a] Veronica S. Sulyaeva,[a] Enrico Benassi,*[b] and Maxim N. Sokolov [a]

Supporting information

Table of contents

Table S1. Experimental details....2

Table S2. Selected geometric parameters (Å, º)....3

Fig. S1. Natural Transition Orbital (NTO) analysis for monomer (upper panel) and model dimer (lower panel) most intense transitions located about 3.521 eV and 3.444 eV respectively. The occupation coefficients are also depicted....4

Fig. S2. DSC data for OP....5

Fig. S3. Experimentally determined dependences of the UCP for YP and the equations of state used for the analysis of thermal expansion tensors....6

Table S3. OLT thermal deformation data....7

Table S4. OHT thermal deformation data....7

Table S5. YP thermal deformation data. Principal axes α_1, α_2, α_3 are parallel to *a*, *b* and *c* unit cell vectors....8

Table S6. Reconstructions of flat sections of reciprocal space at temperatures below (130K) and above (140K) of the OP phase transition....9

Fig. S4. TGA details for OP....10

Table S7. Thermal analysis assignment for OP....10

Fig. S5. TGA details for YP....11

Table S8. Thermal analysis assignment for YP....11

Fig. S6. XRPD data for the solid obtained after thermal decomposition....12

Fig. S7. SEM images of decomposition products....13

Fig. S8. XRPD data for OP....14

Fig. S9. XRPD data for YP....14

Table S1. Experimental details

	OP_subunit	YP	OP_150
Chemical formula	$C_{45}H_{93}Ag_2Mo_8N_9O_{27}$	$C_{42}H_{86}Ag_2Mo_8N_8O_{26}$	$C_{45}H_{93}Ag_2Mo_8N_9O_{27}$
M_r	2175.54	2102.44	2175.54
Crystal system, space group	Triclinic, $P\bar{1}$	Orthorhombic, *Pbca*	Triclinic, $P\bar{1}$
Temperature (K)	84	150	150
a, *b*, *c* (Å)	16.5639 (8), 17.9149 (9), 25.3059 (15)	17.5214 (4), 16.1843 (4), 23.4644 (6)	12.9493 (7), 16.7502 (5), 18.0160 (9)
α, β, γ (°)	104.626 (3), 106.317 (2), 91.236 (2)	90, 90, 90	88.198 (1), 74.295 (1), 68.962 (1)
V (Å^3)	6938.6 (6)	6653.8 (3)	3501.7 (3)
μ (mm^{-1})	2.03	2.11	2.01
Crystal size (mm)	0.10 × 0.04 × 0.02	0.40 × 0.20 × 0.20	0.10 × 0.04 × 0.02
Diffractometer	Bruker D8 Venture	New Xcalibur, AtlasS2	Bruker D8 Venture
Absorption correction	Multi-scan *SADABS* 2016/2: Krause, L., Herbst-Irmer, R., Sheldrick G.M. & Stalke D., J. Appl. Cryst. 48 (2015) 3-10	Multi-scan *CrysAlis PRO* 1.171.38.41 (Rigaku Oxford Diffraction, 2015) Empirical absorption correction using spherical harmonics, implemented in SCALE3 ABSPACK scaling algorithm.	Multi-scan *SADABS* 2016/2: Krause, L., Herbst-Irmer, R., Sheldrick G.M. & Stalke D., J. Appl. Cryst. 48 (2015) 3-10
T_{min}, T_{max}	0.671, 0.746	0.819, 1.000	0.680, 0.746
No. of measured, independent and observed [$I > 2\sigma(I)$] reflections	186187, 38895, 26438	29815, 7762, 6429	46874, 16666, 10696
R_{int}	0.078	0.031	0.101
θ values (°)	θ_{max} = 29.6, θ_{min} = 1.3	θ_{max} = 29.0, θ_{min} = 2.1	θ_{max} = 28.7, θ_{min} = 2.4
$(\sin\theta/\lambda)_{max}$ (Å^{-1})	0.695	0.681	0.676
Range of *h*, *k*, *l*	$-22 \le h \le 22$, $-24 \le k \le 24$, $-35 \le l \le 35$	$-22 \le h \le 23$, $-21 \le k \le 16$, $-19 \le l \le 31$	$-17 \le h \le 17$, $-22 \le k \le 19$, $-24 \le l \le 24$
$R[F^2 > 2\sigma(F^2)]$, $wR(F^2)$, *S*	0.074, 0.170, 1.09	0.024, 0.051, 1.05	0.069, 0.182, 1.10
No. of reflections, parameters, restraints	38895, 1641, 0	7762, 400, 0	16666, 810, 6
H-atom treatment	H-atom parameters constrained	H atoms treated by a mixture of independent and constrained refinement	H-atom parameters constrained
Weighting scheme	$w = 1/[\sigma^2(F_o^2) + 131.5944P]$ where $P = (F_o^2 + 2F_c^2)/3$	$w = 1/[\sigma^2(F_o^2) + (0.0188P)^2 + 3.3072P]$ where $P = (F_o^2 + 2F_c^2)/3$	$w = 1/[\sigma^2(F_o^2) + (0.0429P)^2]$ where $P = (F_o^2 + 2F_c^2)/3$
$\Delta\rho_{max}$, $\Delta\rho_{min}$ (e Å^{-3})	3.31, -2.61	0.52, -0.63	1.79, -1.93

Computer programs: *APEX2* (Bruker-AXS, 2004), *CrysAlis PRO* 1.171.38.41 (Rigaku OD, 2015), *SAINT* (Bruker-AXS, 2004), *SHELXS2014* (Sheldrick, 2014), *SHELXL2014* (Sheldrick, 2014), ShelXle (Hübschle, 2011), CIFTAB-2014 (Sheldrick, 2014).

Table S2. Selected geometric parameters (Å, º)

OP_subunit			
O1—Ag1	2.488 (6)	O42—Ag4	2.519 (6)
O2—Ag1	2.296 (5)	O49—Ag3	2.239 (7)
O3—Ag1	2.540 (6)	N2—Ag1	2.191 (7)
O10—Ag2	2.295 (6)	N5—Ag2	2.197 (7)
O13—Ag2	2.550 (6)	N13—Ag4^{i}	2.578 (8)
O14—Ag2	2.555 (6)	N14—Ag4	2.186 (8)
O30—Ag4	2.234 (7)	N17—Ag3	2.182 (8)
O37—Ag3	2.556 (6)		
N14—Ag4—N13^{i}	104.0 (3)	N14—Ag4—O30	163.5 (3)
N2—Ag1—O1	102.0 (2)	N14—Ag4—O42	109.5 (2)
N2—Ag1—O2	148.6 (2)	O1—Ag1—O3	124.11 (19)
N2—Ag1—O3	122.6 (2)	O2—Ag1—O1	81.5 (2)
N5—Ag2—O10	147.3 (2)	O2—Ag1—O3	76.97 (19)
N5—Ag2—O13	124.2 (2)	O10—Ag2—O13	77.07 (19)
N5—Ag2—O14	102.2 (2)	O10—Ag2—O14	80.5 (2)
N17—Ag3—O37	107.8 (2)	O13—Ag2—O14	122.87 (19)
N17—Ag3—O49	169.6 (3)	O49—Ag3—O37	81.0 (2)
O30—Ag4—N13^{i}	81.6 (2)	O30—Ag4—O42	84.0 (2)
O42—Ag4—N13^{i}	102.0 (2)		
YP			
O1—Ag1	2.2969 (18)	O8—Ag1	2.5746 (17)
O2—Ag1	2.4464 (17)	N2—Ag1	2.188 (2)
N2—Ag1—O1	144.44 (7)	O1—Ag1—O2	78.87 (6)
N2—Ag1—O2	124.41 (7)	O1—Ag1—O8	80.34 (6)
N2—Ag1—O8	105.04 (6)	O2—Ag1—O8	118.67 (5)
OP_150			
O2—Ag1	2.563 (5)	O27—Ag2	2.566 (6)
O3—Ag1	2.305 (6)	N2—Ag1	2.194 (6)
O4—Ag1	2.522 (5)	N5—Ag2	2.189 (7)
O16—Ag2	2.254 (5)		
N2—Ag1—O2	125.4 (2)	O3—Ag1—O2	76.64 (18)
N2—Ag1—O3	147.8 (2)	O3—Ag1—O4	80.36 (19)
N2—Ag1—O4	101.4 (2)	O4—Ag1—O2	121.78 (17)
N5—Ag2—O16	168.4 (3)	O16—Ag2—O27	80.6 (2)
N2—Ag1—O2	125.4 (2)	O3—Ag1—O2	76.64 (18)

Symmetry code(s): (i) -*x*+2, -*y*+1, -*z*+2.

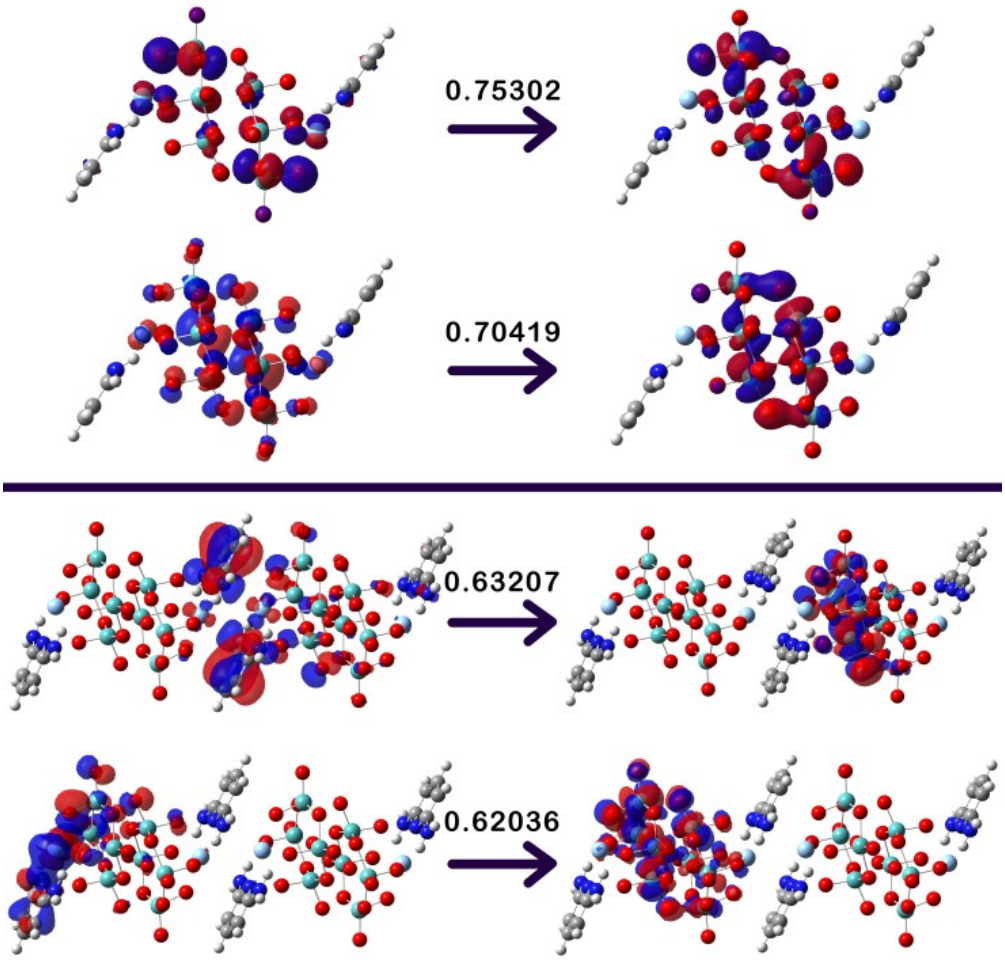

Fig. S1. Natural Transition Orbital (NTO) analysis for monomer (upper panel) and model dimer (lower panel) most intense transitions located about 3.521 eV and 3.444 eV respectively. The occupation coefficients are also depicted.

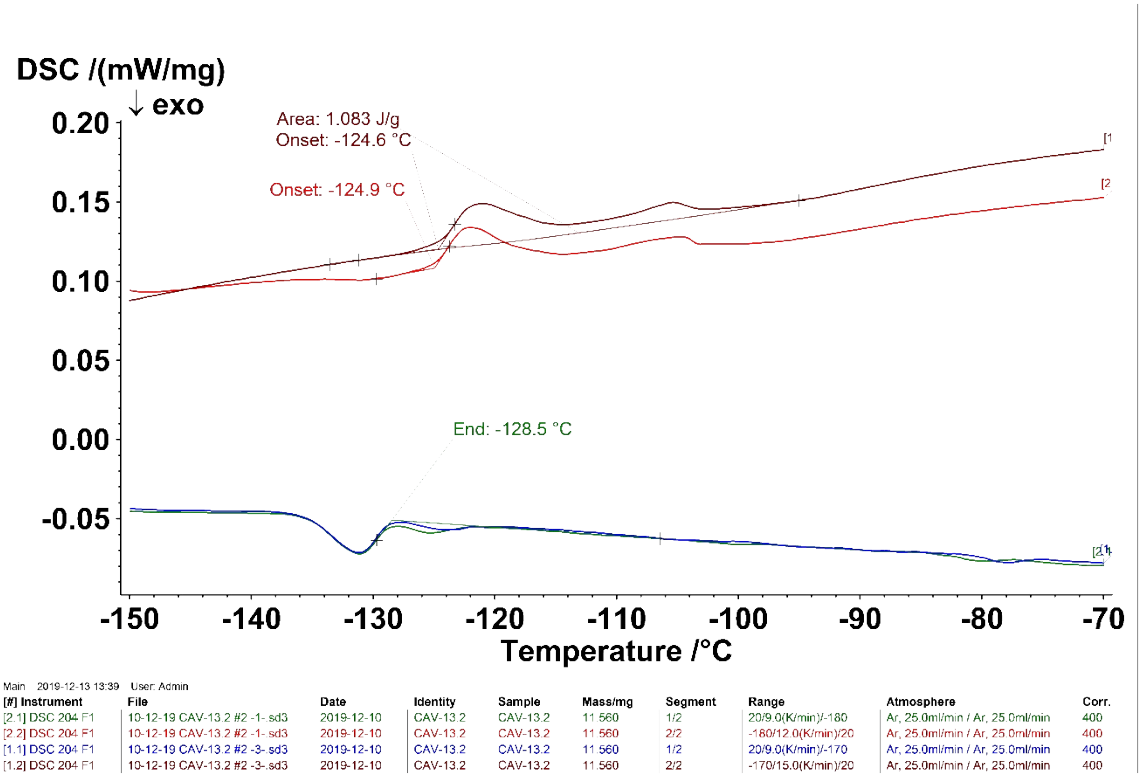

Fig. S2. DSC data for **OP**.

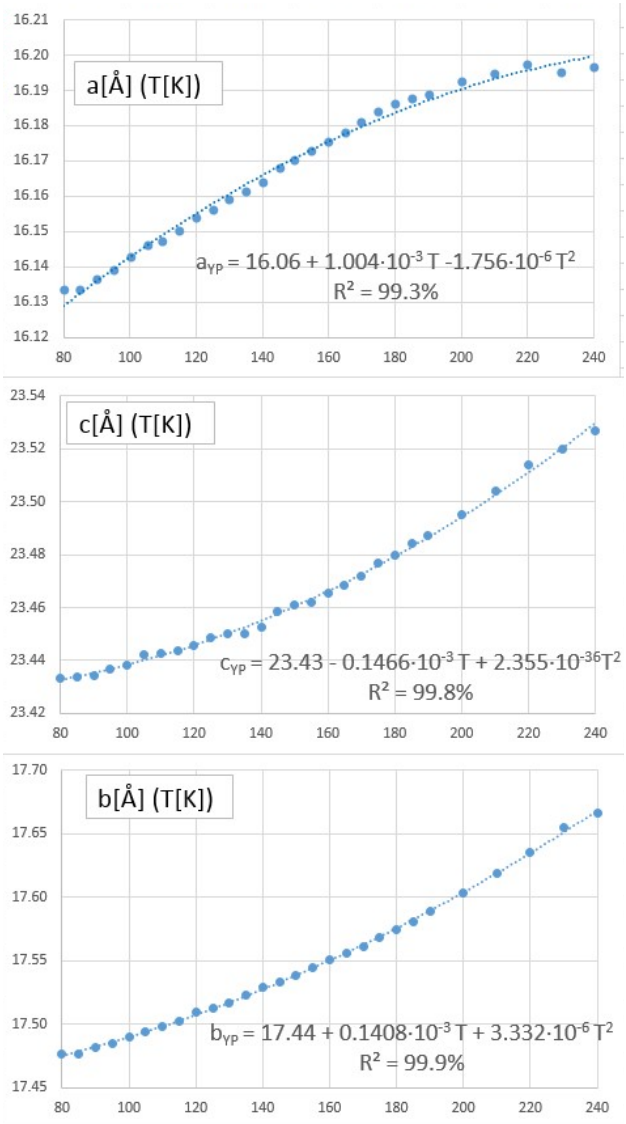

Fig. S3. Experimentally determined dependences of the UCP for YP and the equations of state used for the analysis of thermal expansion tensors.

Values of thermal strain tensor components along the principal axes ($\alpha_i = d(\Delta l/l)/dT$), and their direction angles with the unit cell vectors for the low-temperature red phase (OLT, Table S3), high-temperature red phase (OHT, Table S4), and yellow phase (YP, Table S5).

Table S3. OLT thermal deformation data.

T, K	$\alpha_1\times10^6$, K^{-1}	$\boldsymbol{\alpha_1}$^***a***, *deg*	$\boldsymbol{\alpha_1}$^***b***, *deg*	$\boldsymbol{\alpha_1}$^***c***, *deg*	$\alpha_2\times10^6$, K^{-1}	$\boldsymbol{\alpha_2}$^***a***, *deg*	$\boldsymbol{\alpha_2}$^***b***, *deg*	$\boldsymbol{\alpha_2}$^***c***, *deg*	$\alpha_3\times10^6$, K^{-1}	$\boldsymbol{\alpha_3}$^***a***, *deg*	$\boldsymbol{\alpha_3}$^***b***, *deg*	$\boldsymbol{\alpha_3}$^***c***, *deg*
90	**106.0**	70.6	31.8	57.9	**59.1**	62.6	65.6	38.9	**-59.2**	34.5	70.9	70.5
95	**106.0**	70.6	31.8	57.8	**59.1**	62.6	65.7	38.9	**-59.2**	34.6	70.9	70.5
100	**106.0**	70.6	31.8	57.8	**59.1**	62.6	65.7	38.9	**-59.3**	34.6	70.9	70.5
105	**106.0**	70.6	31.8	57.8	**59.0**	62.6	65.7	38.9	**-59.3**	34.6	70.9	70.5
110	**106.0**	70.6	31.8	57.8	**59.0**	62.6	65.7	38.9	**-59.4**	34.6	70.9	70.5
115	**106.0**	70.6	31.8	57.8	**58.9**	62.5	65.7	38.9	**-59.4**	34.6	70.9	70.6
120	**106.0**	70.6	31.8	57.8	**58.9**	62.5	65.7	38.9	**-59.5**	34.7	70.9	70.6
125	**106.0**	70.6	31.7	57.8	**58.9**	62.5	65.7	38.9	**-59.5**	34.7	70.9	70.6
130	**106.0**	70.6	31.7	57.8	**58.8**	62.5	65.7	38.9	**-59.5**	34.7	70.9	70.6

Table S4. OHT thermal deformation data.

T, K	$\alpha_1\times10^6$, K^{-1}	$\boldsymbol{\alpha_1}$^***a***, *deg*	$\boldsymbol{\alpha_1}$^***b***, *deg*	$\boldsymbol{\alpha_1}$^***c***, *deg*	$\alpha_2\times10^6$, K^{-1}	$\boldsymbol{\alpha_2}$^***a***, *deg*	$\boldsymbol{\alpha_2}$^***b***, *deg*	$\boldsymbol{\alpha_2}$^***c***, *deg*	$\alpha_3\times10^6$, K^{-1}	$\boldsymbol{\alpha_3}$^***a***, *deg*	$\boldsymbol{\alpha_3}$^***b***, *deg*	$\boldsymbol{\alpha_3}$^***c***, *deg*
150	**103.0**	35.8	67.4	40.1	**36.9**	87.7	24.2	78.9	**13.1**	54.3	81.8	52.1
155	**103.0**	35.2	66.9	40.7	**36.0**	89.5	23.3	75.3	**11.6**	54.8	86.9	53.1
160	**102.0**	34.7	66.4	41.3	**35.5**	87.1	23.6	71.9	**9.8**	55.5	88.4	54.3
165	**102.0**	34.1	65.9	42.0	**35.4**	85.2	24.8	68.9	**7.5**	56.3	84.3	55.7
170	**101.0**	33.6	65.4	42.7	**35.4**	83.7	26.5	66.2	**5.0**	57.2	80.9	56.9
175	**101.0**	33.0	64.8	43.4	**35.7**	82.6	28.3	64.0	**2.3**	58.0	78.0	58.1
180	**101.0**	32.5	64.2	44.1	**36.1**	82.0	30.0	62.0	**-0.6**	58.8	75.7	59.1
185	**100.0**	31.9	63.6	44.9	**36.6**	81.6	31.7	60.2	**-3.6**	59.4	73.7	59.9
190	**100.0**	31.4	62.9	45.7	**37.2**	81.4	33.3	58.6	**-6.6**	60.1	72.1	60.7
195	**100.0**	30.9	62.3	46.5	**37.7**	81.4	34.8	57.1	**-9.8**	60.6	70.8	61.3
200	**99.8**	30.3	61.5	47.3	**38.4**	81.6	36.2	55.7	**-13.0**	61.1	69.6	61.8
205	**99.6**	29.8	60.8	48.2	**39.0**	81.9	37.5	54.4	**-16.3**	61.5	68.6	62.3
210	**99.5**	29.3	60.1	49.1	**39.6**	82.3	38.8	53.1	**-19.6**	61.9	67.8	62.7

Table S5. YP thermal deformation data. Principal axes α_1, α_2, α_3 are parallel to *a*, *b* and *c* unit cell vectors.

T, K	$\alpha_1 \times 10^6$, K^{-1}	$\alpha_2 \times 10^6$, K^{-1}	$\alpha_3 \times 10^6$, K^{-1}
80	44.7	38.7	9.2
90	42.5	42.5	11.2
100	40.3	46.3	13.1
110	38.1	50.1	15.0
120	35.9	53.9	16.9
130	33.8	57.7	18.8
140	31.6	61.4	20.8
150	29.4	65.2	22.7
160	27.2	68.9	24.6
170	25.0	72.7	26.5
180	22.9	76.4	28.4
190	20.7	80.1	30.3
200	18.5	83.8	32.2
210	16.3	87.6	34.2
220	14.2	91.3	36.1
230	12.0	94.9	38.0
240	9.8	98.6	39.9
250	7.7	102.0	41.8
260	5.5	106.0	43.7
270	3.3	110.0	45.6
280	1.2	113.0	47.5

Table S6. Reconstructions of flat sections of reciprocal space at temperatures below (130K) and above (140K) of the OP phase transition.

Circles indicate the positions of reflections from the high-temperature lattice (subcell). At 130 K, superstructure reflections associated with a doubling of the parameter a (half-integer values of *h* in the lattice of the high-temperature phase) are clearly observed. At 140 K, there are weaker non-Bragg peaks that deviate significantly from half-integer values of *h*, the appearance of which is probably caused by pre-transition phenomena in the high-temperature phase

	130 K	140 K
*h*0*l*	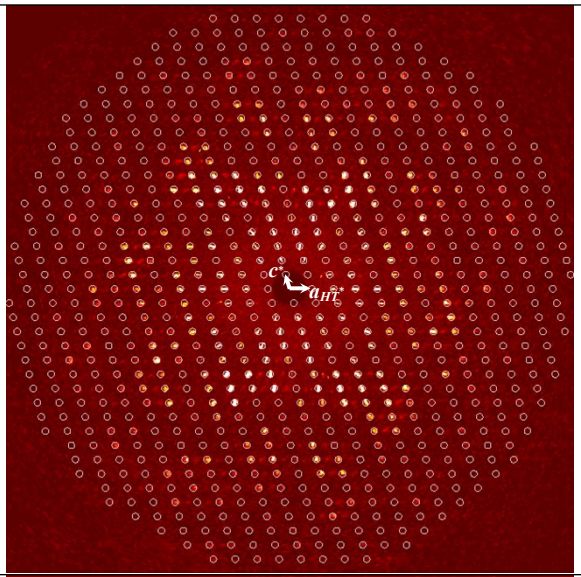	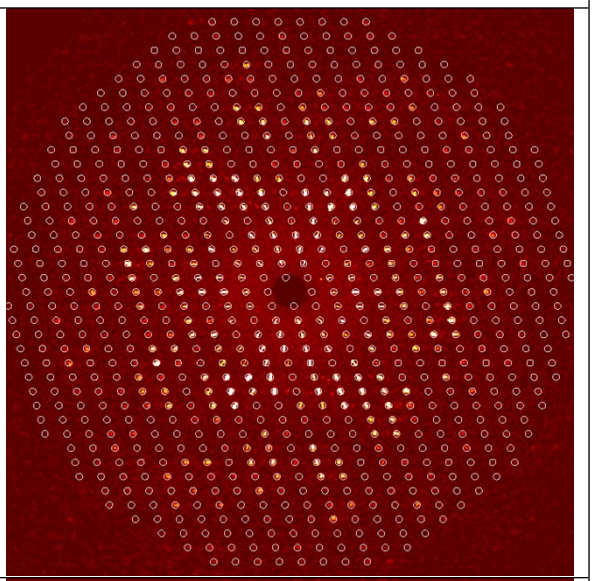
*h*5*l*	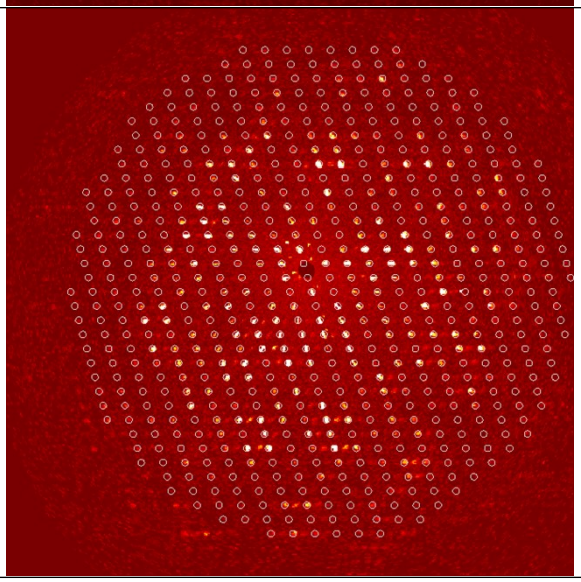	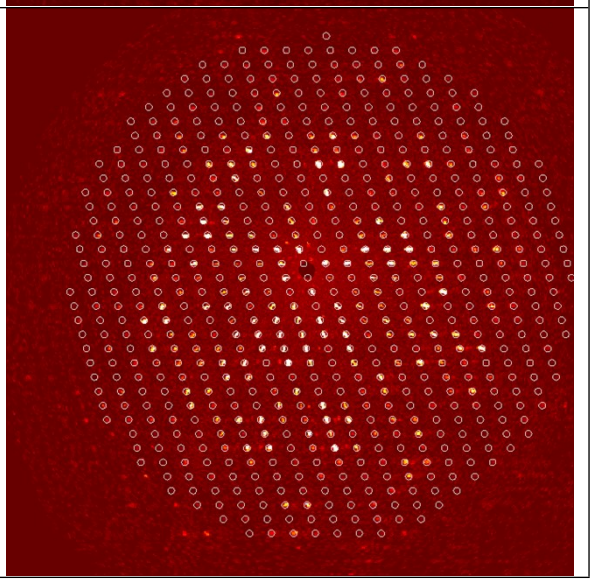

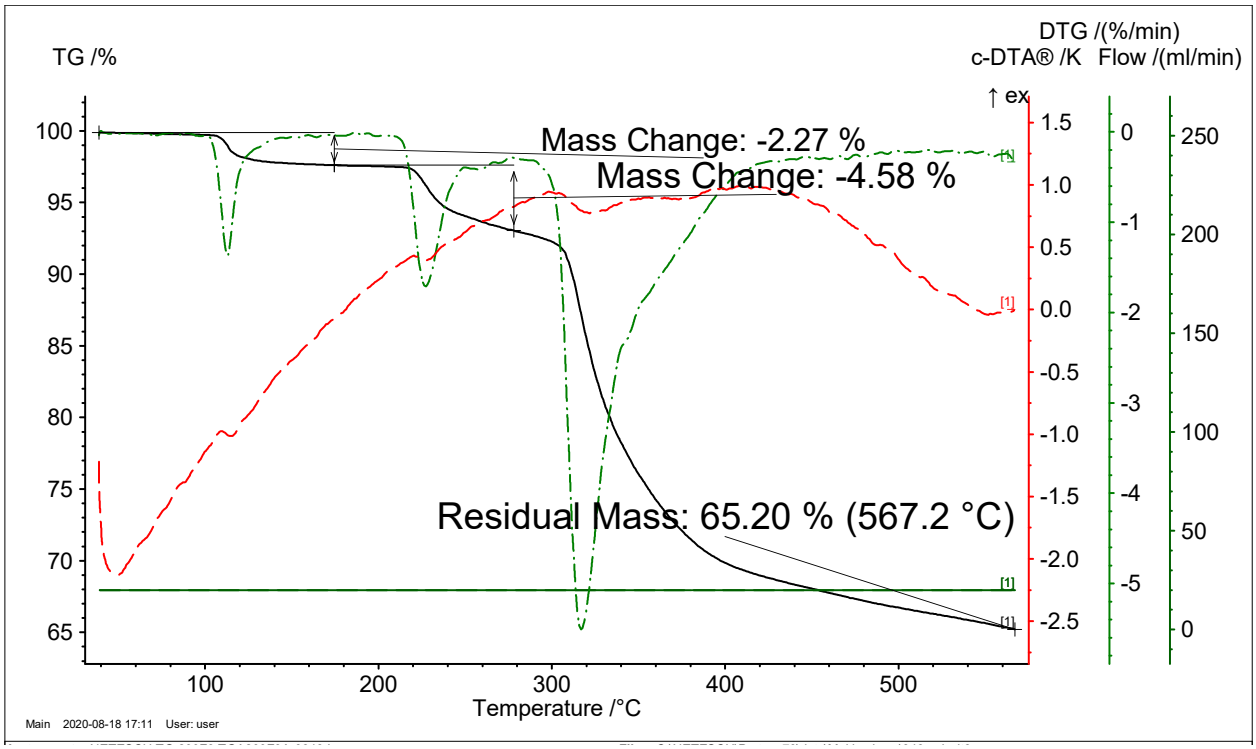

Fig. S4. TGA details for OP

Table S7. Thermal analysis assignment for OP

Mass loss	Assignment	Molar mass loss
2.27	0.7DMF	50
4.58	0.3DMF + 0.6 N_2-Py	109
27.95	1.4N_2-Py + 2Bu_3N + 2butene-1 + 0.7O_2	634.6
Residual mass – 65.20%	$Ag_2Mo_4O_{13}$+MoO_3 + Ag + 0.3O_2	

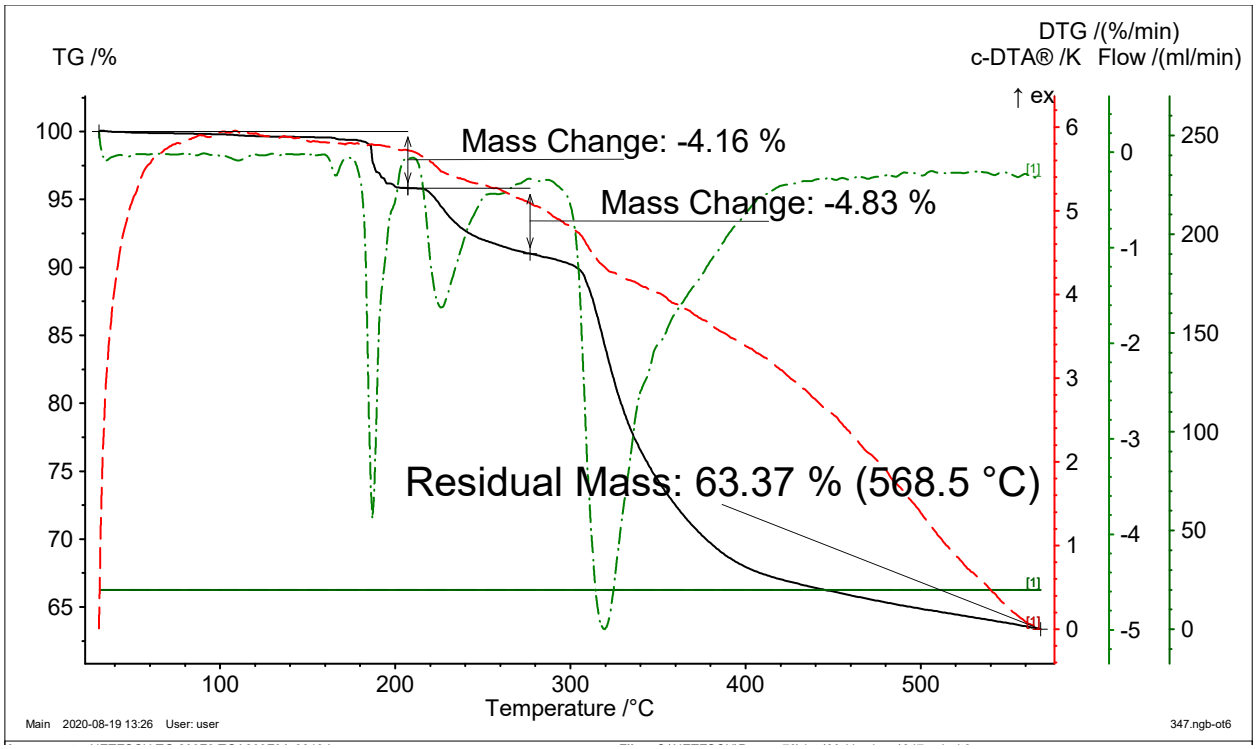

Fig. S5. TGA details for YP

Table S8. Thermal analysis assignment for YP

Mass loss	Assignment	Molar mass loss
4.16	0.8 N_2-Py	88
4.83	N_2-Py	102.2
27.64	0.2N_2-Py + 2Bu_3N + 2butene-1 + xO_2	505.8+x32
Residual mass – 63.37%	$Ag_2Mo_4O_{13}$+MoO_3 + Ag + xO_2	

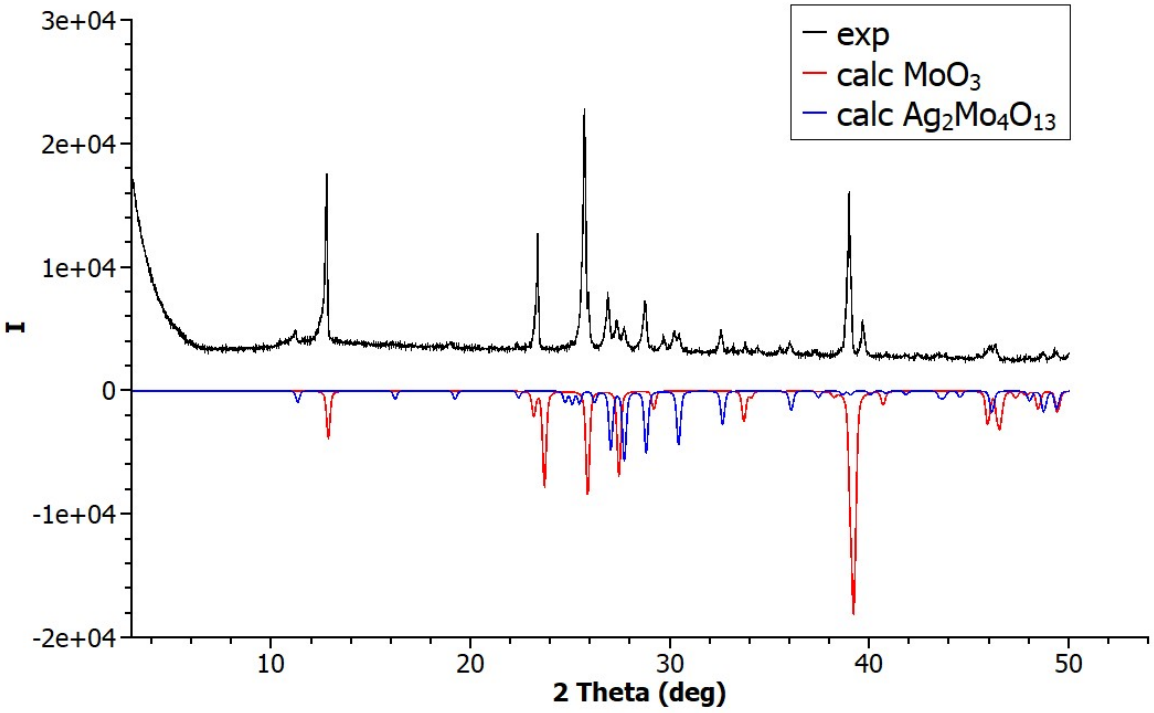

Fig. S6. XRPD data for the solid obtained after thermal decomposition

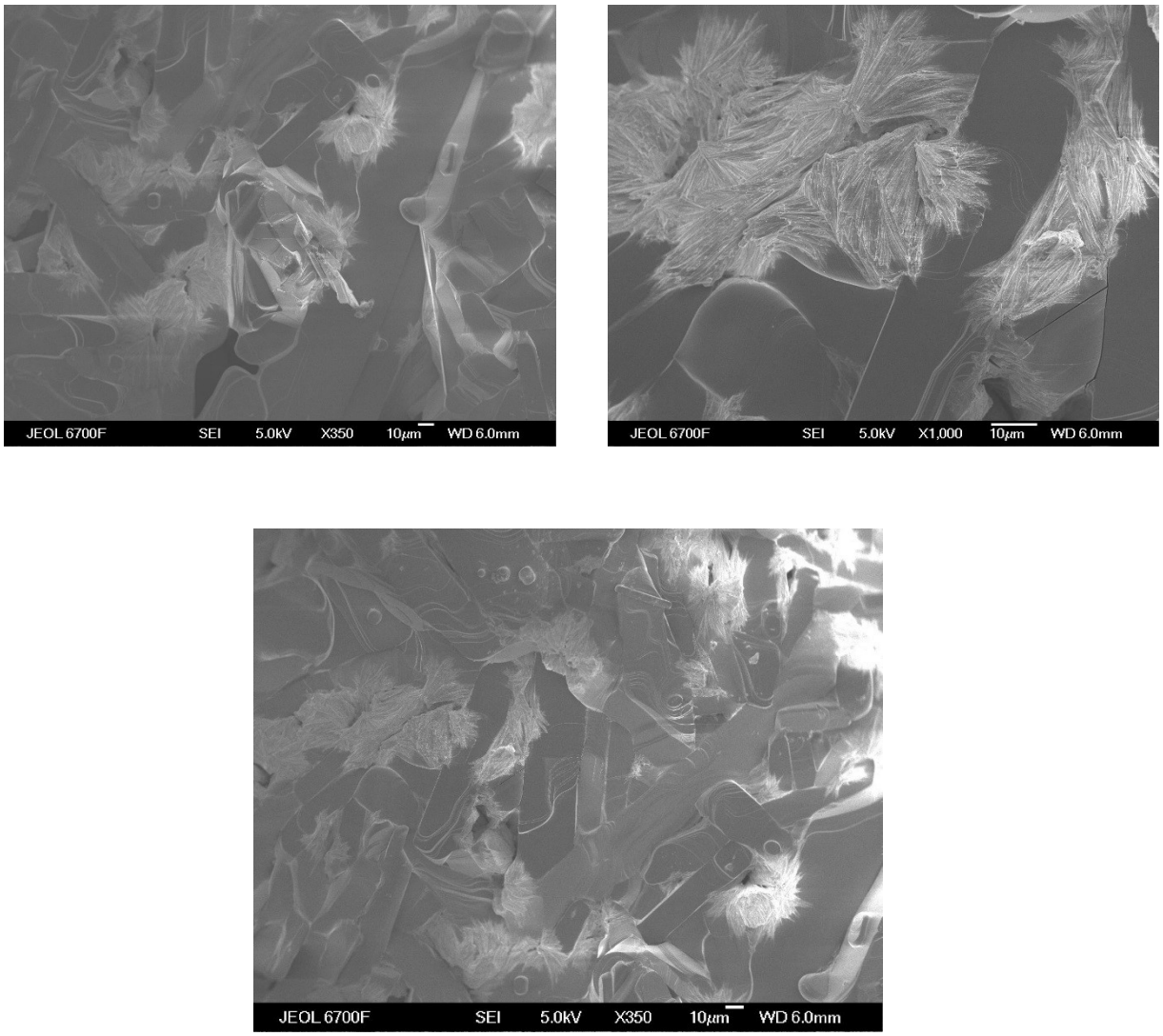

Fig. S7. SEM images of decomposition products.

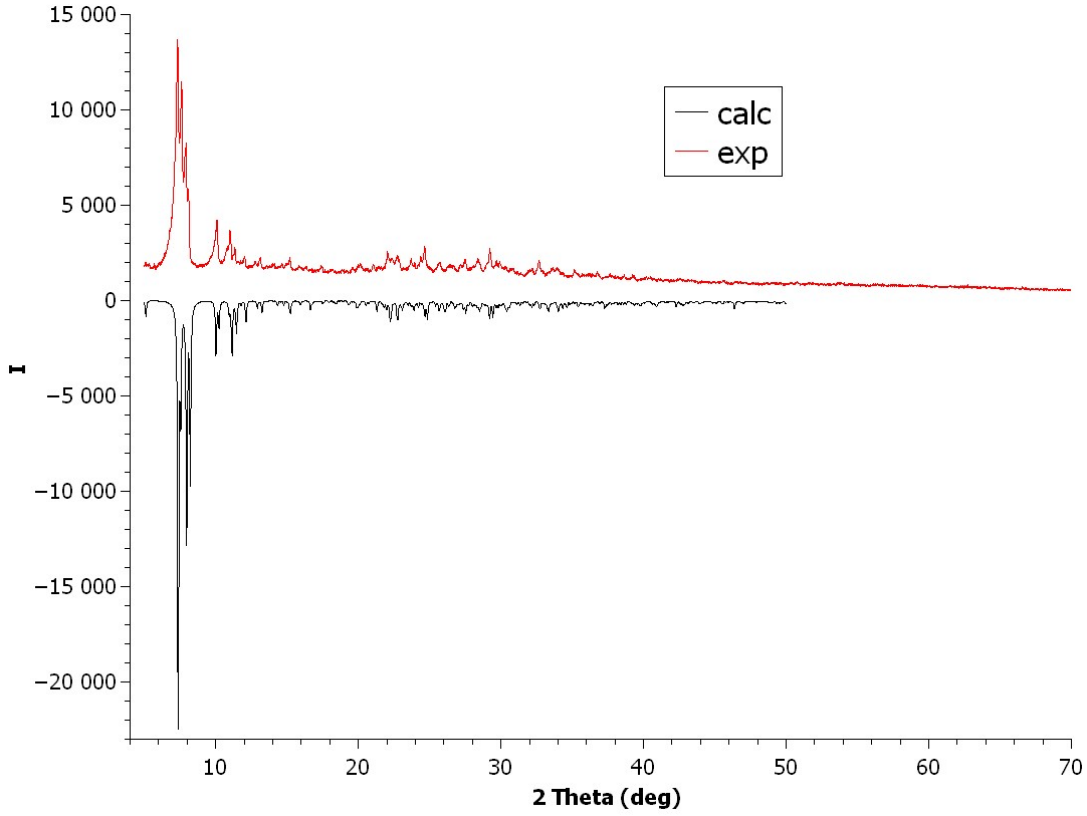

Fig. S8. XRPD data for OP.

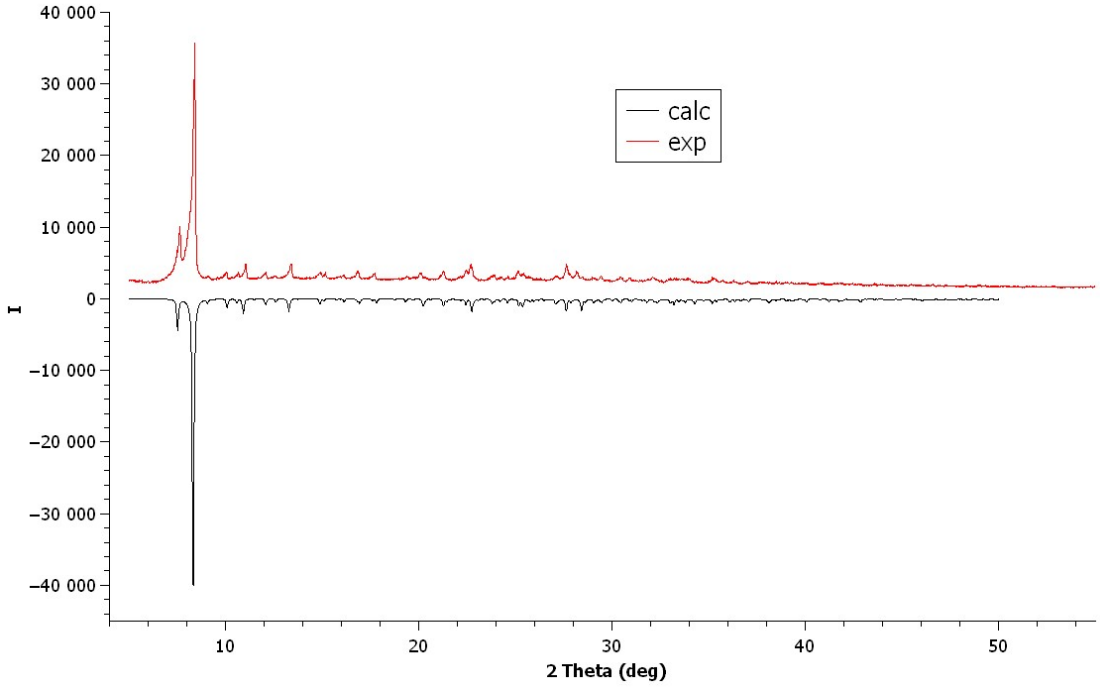

Fig. S9. XRPD data for YP.